Electronic Supplementary Material (ESI) for Journal of Materials Chemistry C.

Molecular Properties Controlling Chirality Transfer to Halide Perovskite: Computational Insights

Aaron Forde[1,2], Amanda C. Evans[3], Wanyi Nie[4], Sergei Tretiak[1,4], Amanda J Neukirch[1]

[1]*Theoretical Division, Los Alamos National Laboratory, Los Alamos, New Mexico 87545, United States*

[2]*Center for Nonlinear Studies, Los Alamos National Laboratory, Los Alamos, New Mexico 87545, United States*

[3]*Materials Science and Technology Division, Los Alamos National Laboratory, Los Alamos, New Mexico 87545, United States*

[4]*Center for Integrated Nanotechnologies, Los Alamos National Laboratory, Los Alamos, New Mexico 87545, United States*

*Corresponding Authors: Aaron Forde (aforde@lanl.gov) and Amanda Neukirch (ajneukirch@lanl.gov)

Supplemental Figures

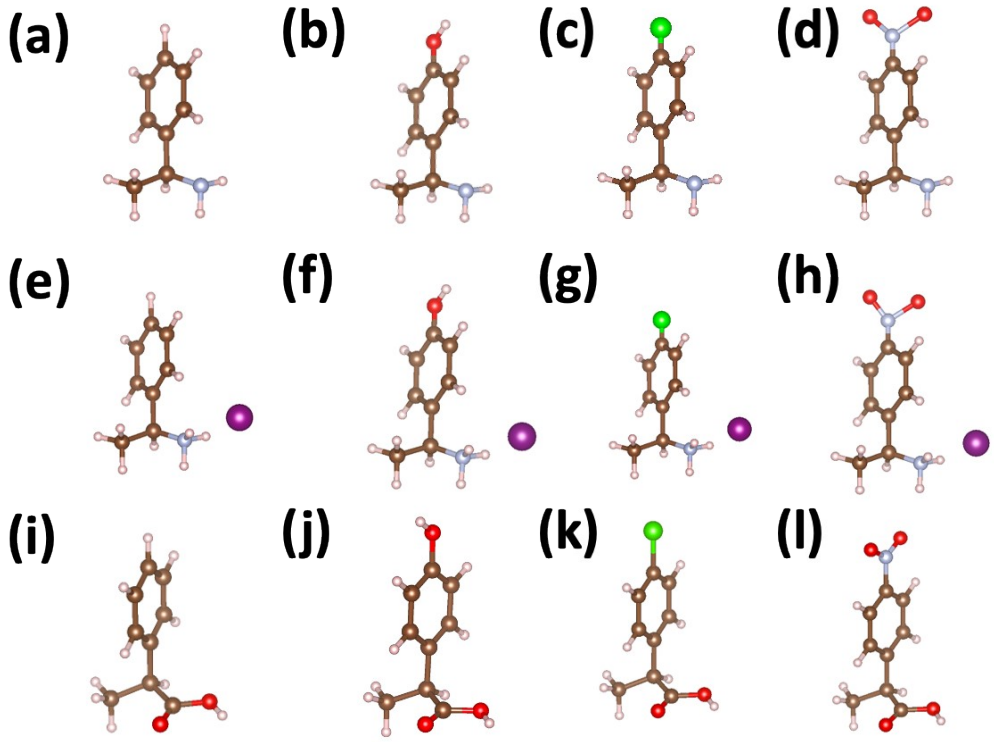

Figure S1: (a)-(d) Atomistic models of methylbenzylamines functionalized with **(a)**H, **(b)** OH, **(c)** Cl, and **(d)** NO2 groups at the *meso* position of the aryl group. **(e)-(h)** Atomistic models of methylbenzylammonium iodide functionalized with **(e)** H, **(f)** OH, **(g)** Cl, and **(h)** NO2 groups at the *meso* position of the aryl group. **(i)-(l)** Atomistic models of methylphenyl acetic acid functionalized with **(i)** H, **(j)** OH, **(k)** Cl, and **(l)** NO2 groups at the *meso* position of the aryl group

Table S1: Lowest energy transition energies and ground-state static dipole moment for isolated aryl-functionalized (R)-MBA, (R)-MBAmm, and R-MPAc molecules and when bound to $CsPbI_3$ cluster surface

	E_{gap}(eV)	$\|\vec{\mu}\|$ (Debye)	μ_x	μ_y	μ_z
CsPbI3 cluster + Chiral Molecules					
R, MBA - OH	4.30	2.87	-2.45	1.50	-0.02
R, MBA - H	4.30	2.53	2.39	-0.05	-0.81
R, MBA - Cl	4.30	2.85	-0.57	1.83	-2.11
R, MBA - NO2	4.02	5.35	1.80	3.72	-3.39
R, MBAmmI - OH	4.30	2.76	0.79	-2.59	0.56
R, MBAmm - H	4.30	3.53	-0.25	-2.81	-2.11
R, MBAmmI - Cl	4.30	3.17	1.69	-1.70	-2.08
R, MBAmmI - NO2	4.02	5.26	4.75	-0.56	-2.19
R,MPAc-OH	4.23	3.36	3.02	-0.75	-1.27
R,MPAc-H	4.23	4.56	3.79	1.99	1.57
R,MPAc-Cl	4.23	5.57	5.11	-2.18	0.30
R,MPAc-NO2	4.02	7.95	7.16	-2.15	2.71
Chiral Molecules					
R, MBA - OH	5.09	1.19	-1.08	-0.35	-0.37
R, MBA	5.43	1.62	0.80	-1.18	-0.76
R, MBA - Cl	5.33	4.07	-3.75	1.30	-0.89
R, MBA - NO2	4.02	7.10	6.88	-1.43	-0.99
R, MBAmmI - OH	5.16	11.55	8.53	7.69	1.17
R, MBAmmI - H	5.26	13.02	10.82	7.01	1.84
R, MBAmmI - Cl	5.19	13.11	5.93	11.55	1.85
R, MBAmmI - NO2	4.01	14.01	2.22	13.79	1.07
R, MPAc - OH	5.08	0.63	0.84	-0.16	1.31
R,MPAc – H	5.42	1.85	1.04	1.20	0.95
R, MPAc – C	5.28	2.32	1.33	1.87	-0.35
R,MPAc – NO2	4.02	5.38	-4.86	-2.30	-0.36

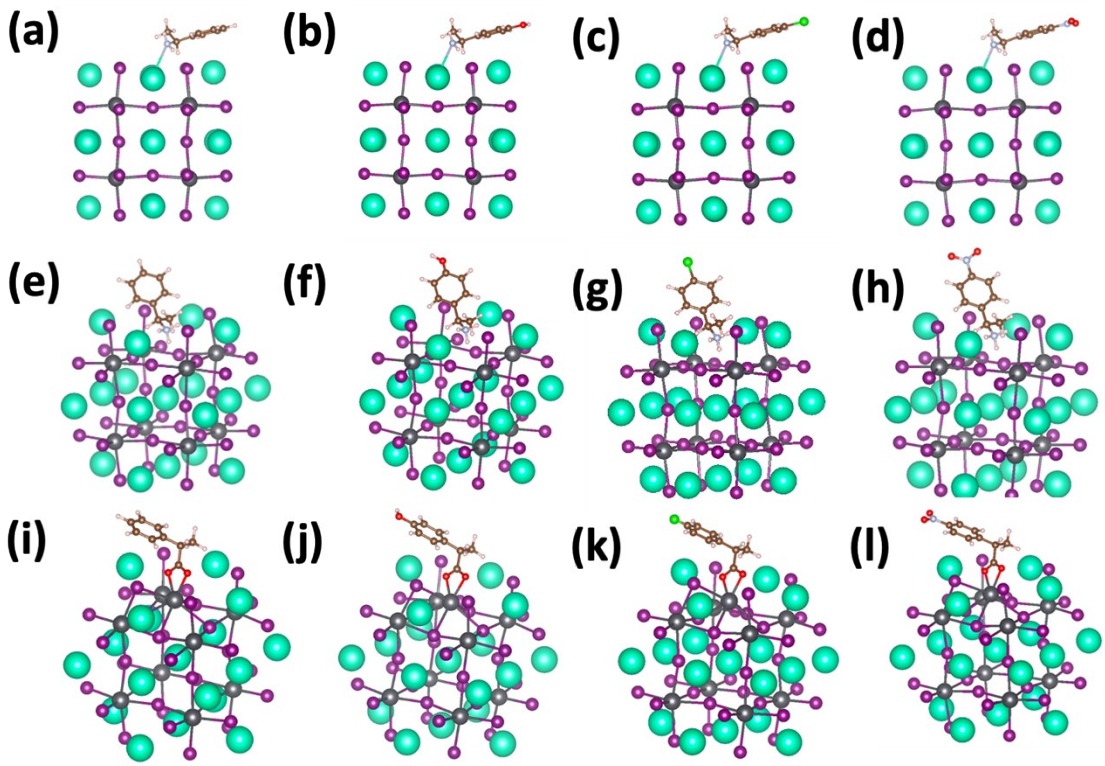

Figure S2: (a)-(d) Atomistic models of (R)-MBA functionalized with **(a)** H, **(b)** OH, **(c)** Cl, and **(d)** NO2 groups coordinated to surface Cs ion of the CsPbI3 cluster. **(e)-(h)** Atomistic models of (R)-MBAmm^{+} functionalized with **(e)** H, **(f)** OH, **(g)** Cl, and **(h)** NO2 groups occupying a surface A^{+} cation site of the perovskite cluster. Atomistic models of (R)-MPAc^{-} functionalized with **(e)** H, **(f)** OH, **(g)** Cl, and **(h)** NO2 groups bound to a Pb^{2+} defect occupying the A^{+} cation site.

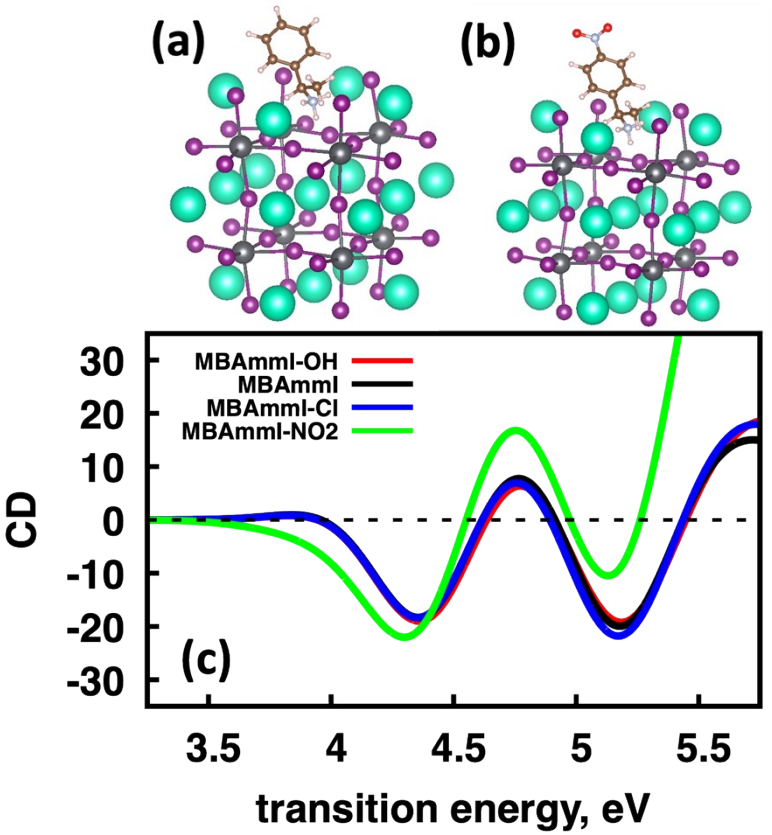

Figure S3: Impact of functionalizing the aryl-group of the chiral molecule with electron donating and withdrawing groups on the circular dichroism spectra. **(a)** Atomistic models for (R)-MBAmmI-H and **(b)** (R)-MBAmmI-NO_2. **(c)** Circular dichroism spectra for (R)-MBAmmI-H binding to the CsPbI3 cluster (black) and functionalizing with OH (red), Cl (blue), and NO_2 (green) groups.

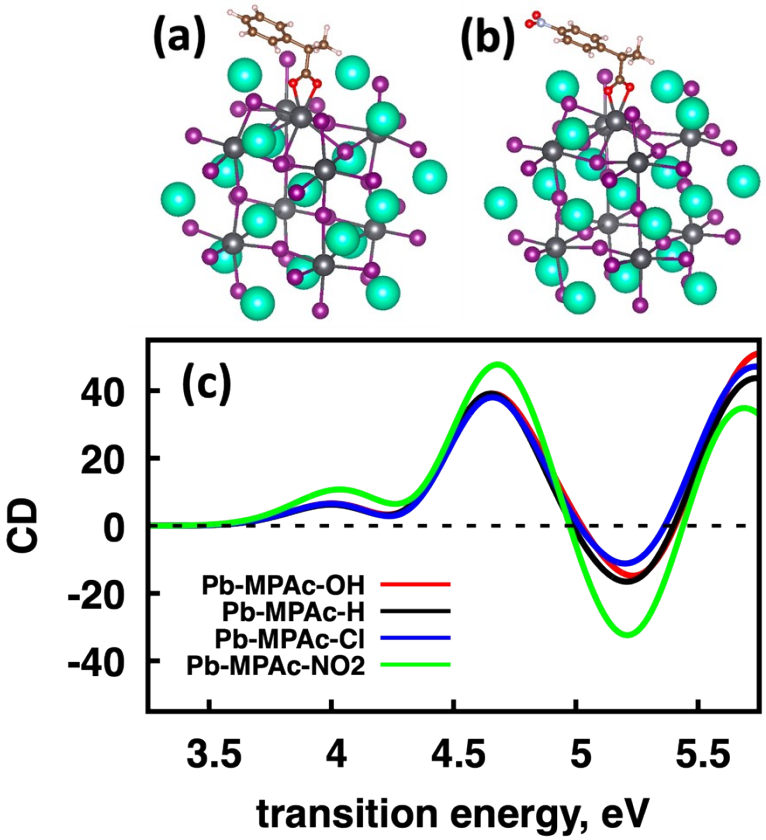

Figure S4: Impact of functionalizing the aryl-group of the chiral molecule with electron donating and withdrawing groups on the circular dichroism spectra. **(a)** Atomistic models for (R)-MPAc-H and **(b)** (R)- MPAc -NO_2. **(c)** Circular dichroism spectra for (R)- MPAc -H binding to the CsPbI3 cluster (black) and functionalizing with OH (red), Cl (blue), and NO_2 (green) groups.

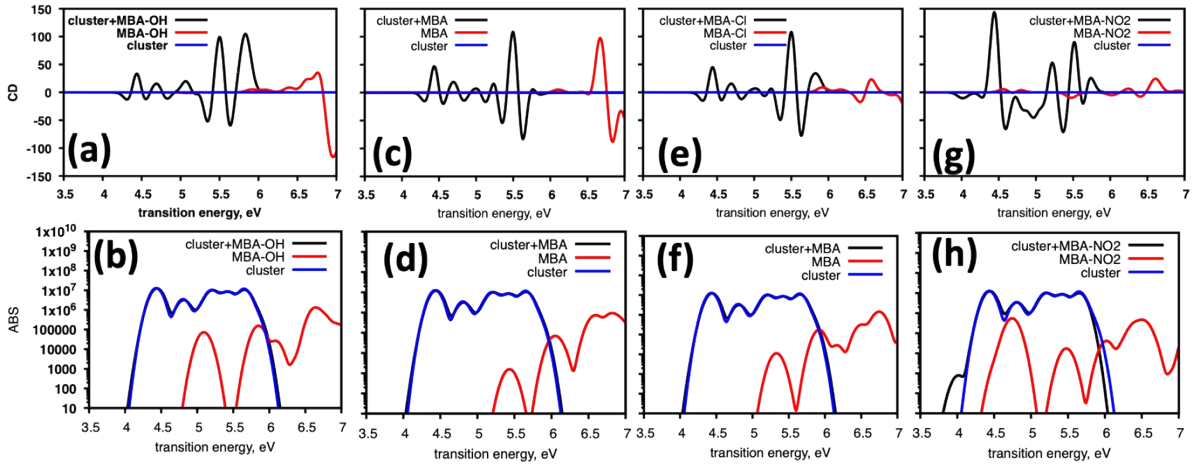

Figure S5: Overlay of circular dichroism and absorption spectra for the joint system (black), isolated cluster (blue), and isolated chiral molecule (red) for **(a)-(b)** OH, **(c)-(d)** H, **(e)-(f)** Cl, and **(g)-(h)** NO2 functionalization of the *meso* postion of the aryl group of MBA.

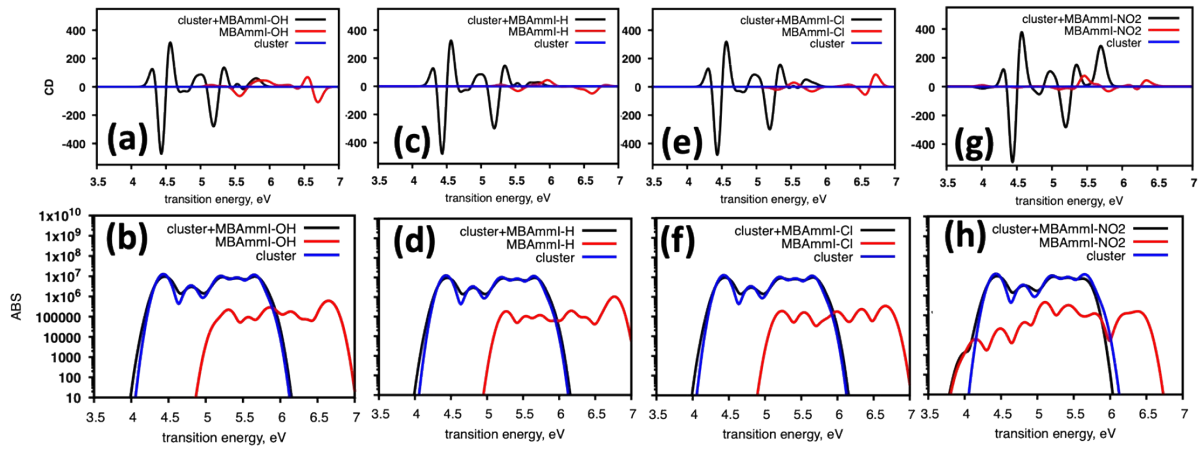

Figure S6: Overlay of circular dichroism and absorption spectra for the joint system (black), isolated cluster (blue), and isolated chiral molecule (red) for **(a)-(b)** OH, **(c)-(d)** H, **(e)-(f)** Cl, and **(g)-(h)** NO2 functionalization of the *meso* postion of the aryl group of MBAmm.

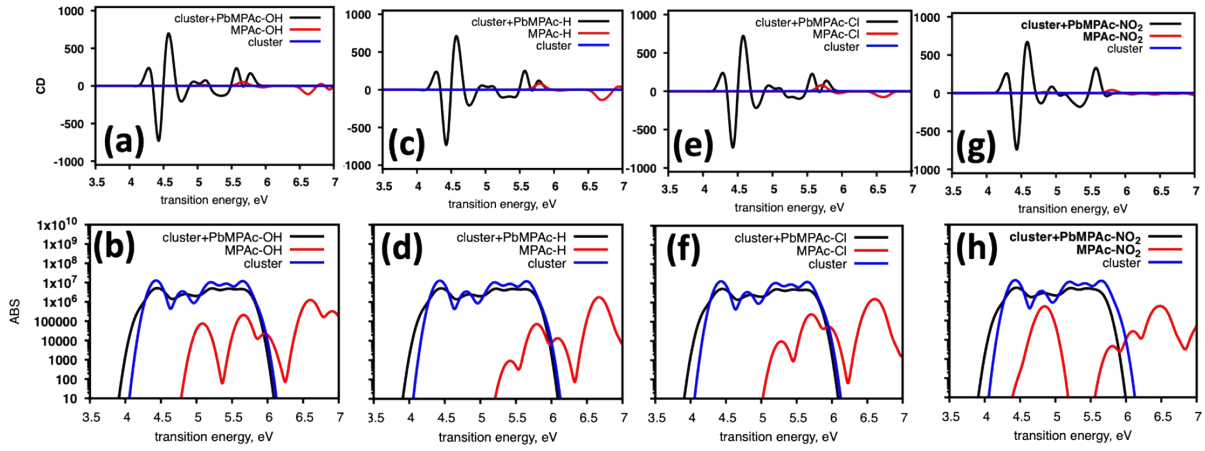

Figure S7: Overlay of circular dichroism and absorption spectra for the joint system (black), isolated cluster (blue), and isolated chiral molecule (red) for **(a)-(b)** OH, **(c)-(d)** H, **(e)-(f)** Cl, and **(g)-(h)** NO2 functionalization of the *meso* postion of the aryl group of MPAc.

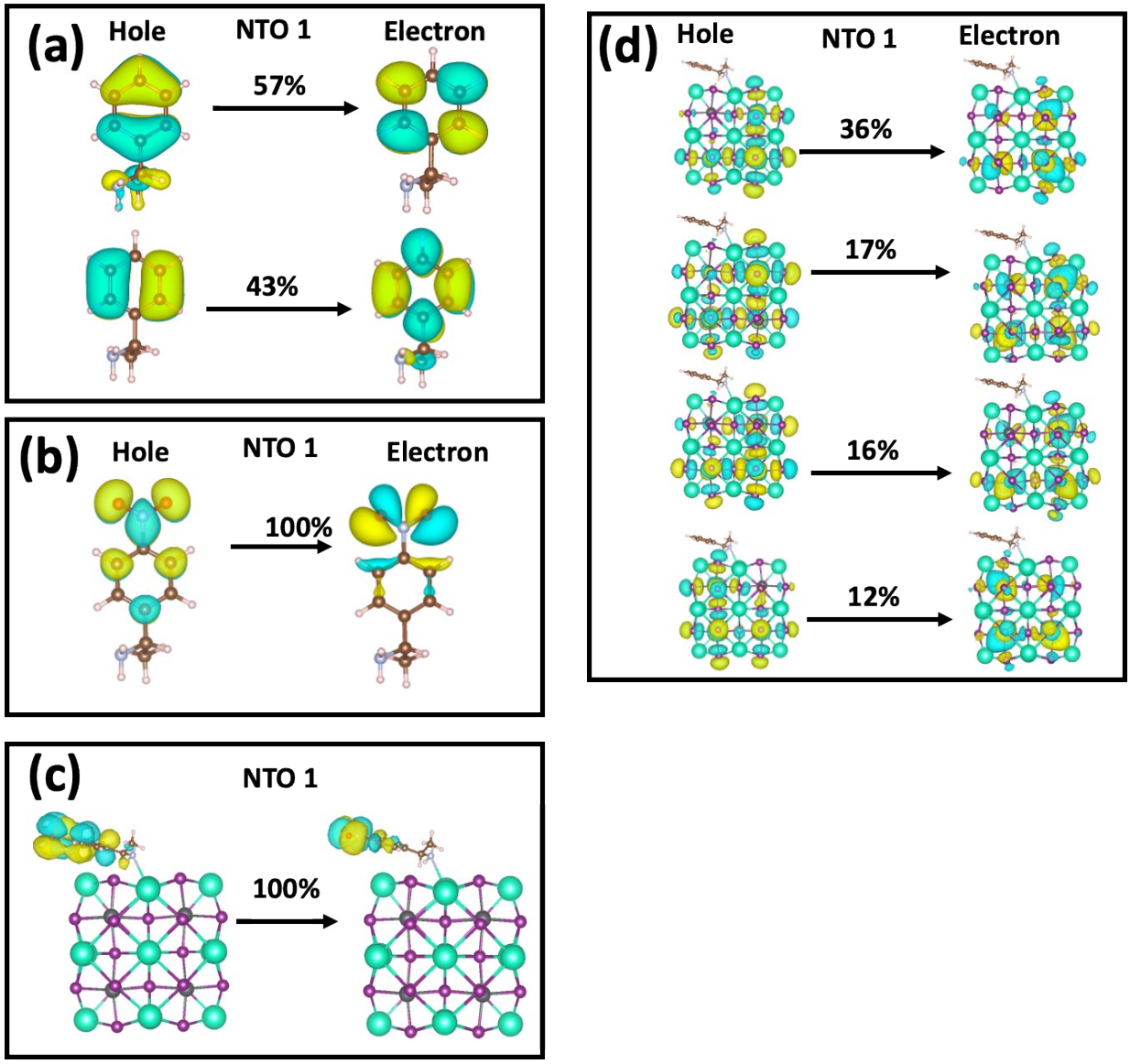

Figure S8: Natural transition orbitals corresponding to the lowest energy excitations for **(a)** MBA-H, **(b)** MBA-NO2, **(c)** MBA-NO2 coordinated to the surface Cs of the perovskite cluster, and **(d)** MBA-H coordinated to the surface Cs of the perovskite cluster. Note that the NO_2 group in **(c)** introduces a transition below the optical bandgap of the $CsPbI_3$ cluster.

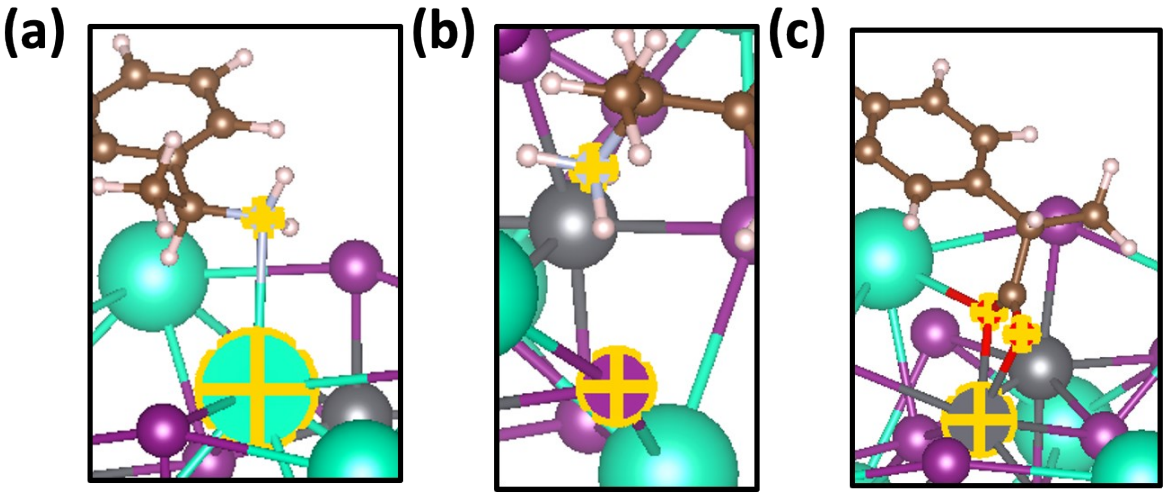

Figure S9: Visualization of the atoms selected to compare Bader charges between unfunctionalized and funcitionalized aryl groups with NO_2 for **(a)** the nitrogen (grey) and Cs^+ (teal) surface cation, **(b)** nitrogen (grey) and hydrogen-bond coordinated I^- surface ion (purple), and **(c)** oxygen (red) and surface cation Pb^{2+} (grey).

Table S2: Bader charges associated with atoms which are involved at the molecule-perovskite interface

Model	Atom 1	Charge	Atom2	Charge	Atom3	Charge
R, MBA-H	N	6.19	Cs	8.16	x	x
R, MBA - NO2	N	6.16	Cs	8.16	x	x
R, MBAmmI-H	N	6.16	I	7.68	x	x
R, MBAmmI - NO2	N	6.22	I	7.69	x	x
R,MPAc-H	O1	7.14	O2	7.16	Pb	2.89
R,MPAc-NO2	O1	7.15	O2	7.17	Pb	2.89

Table S3: Values of transition energy, rotatory strength, and oscillator strength for excited-states which have highest intensity contribution to main peaks in CD spectrum

	Transition Energy, eV	Rot_vel	OS
NTO	**(R)-MBA-H**		
1	4.30	-0.91	0.001
8	4.46	592.88	0.051
11	4.48	-950.80	0.524
NTO	**(R)-MBA-NO2**		
2	4.30	-1.39	0.002
9	4.46	1122.28	0.143
12	4.48	-573.48	0.358

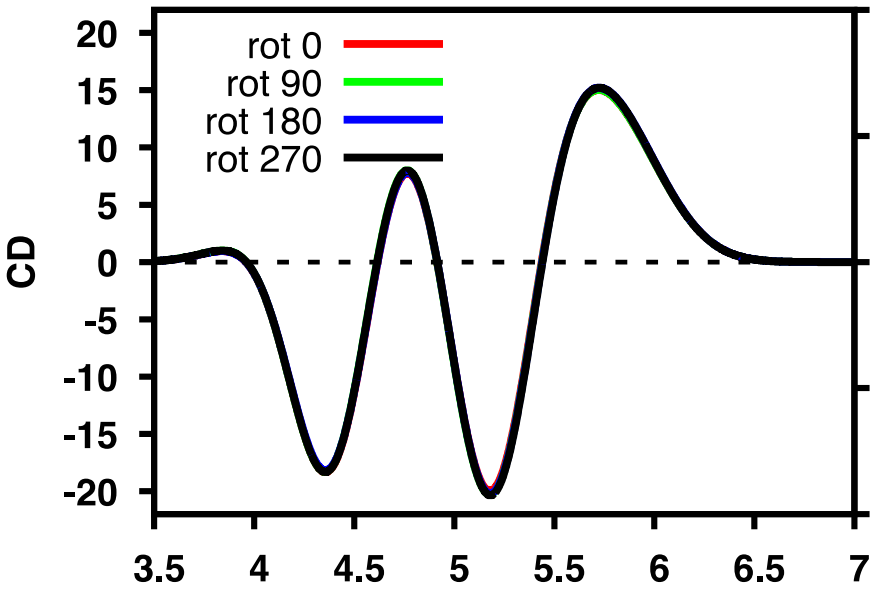

Figure S10: Rotation of the of (R)-MBAmm^{+}-H ligand on the $CsPbI_3$ cluster surface and the resultant CD spectra. We see that regardless of initial condition the CD remains unchanged. This removes the need for conformational averaging of the chiral aryl molecules on the surface.

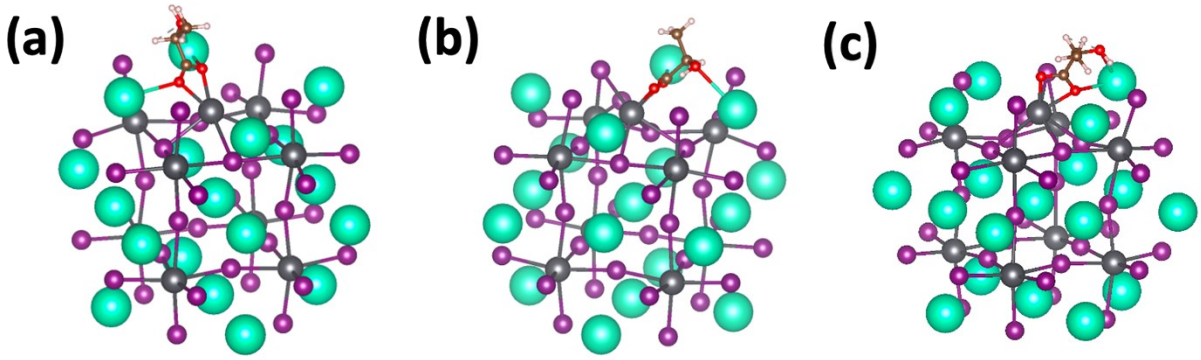

Figure S11: (a)-(c) Pb-rich CsPbI3 cluster with lactate binding to the surface Pb defect in different configurations.

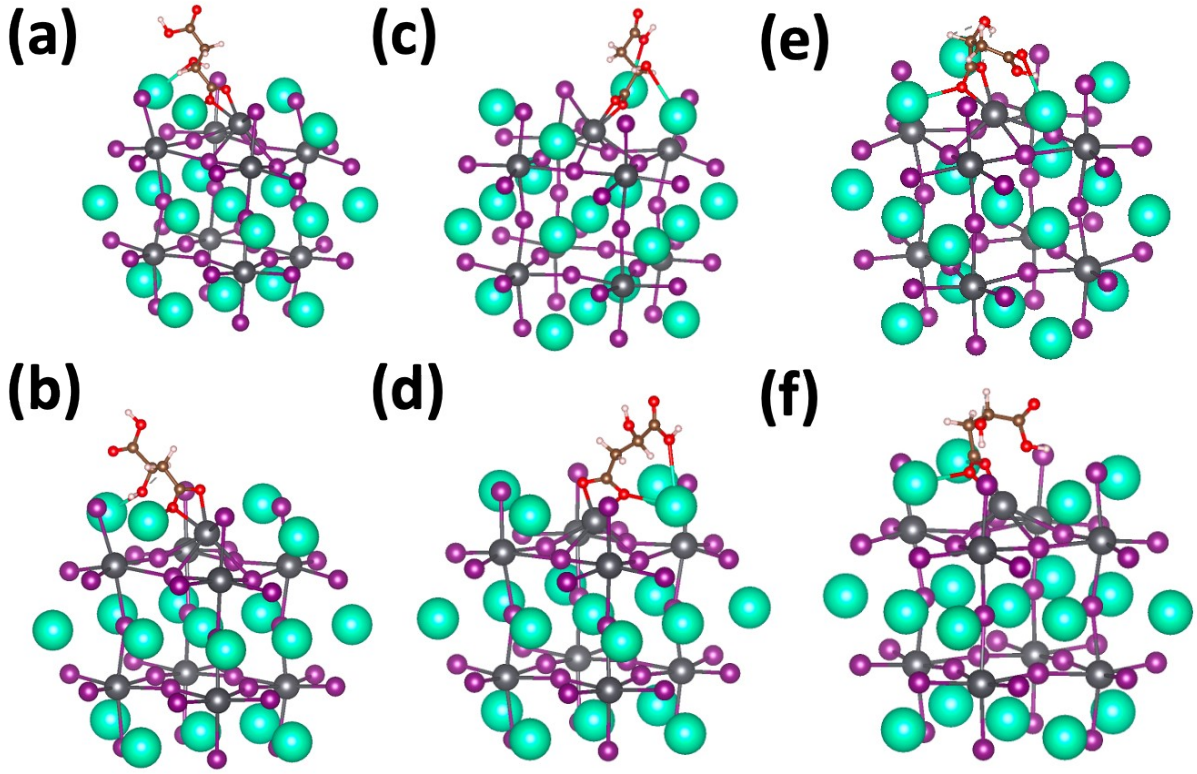

Figure S12: Pb-rich CsPbI3 cluster with malate binding to the surface Pb defect in the **(a)-(b)** trans, **(c)-(d)** gaunche(-), and **(e)-(f)** gaunche(+) conformations as initial conditions.

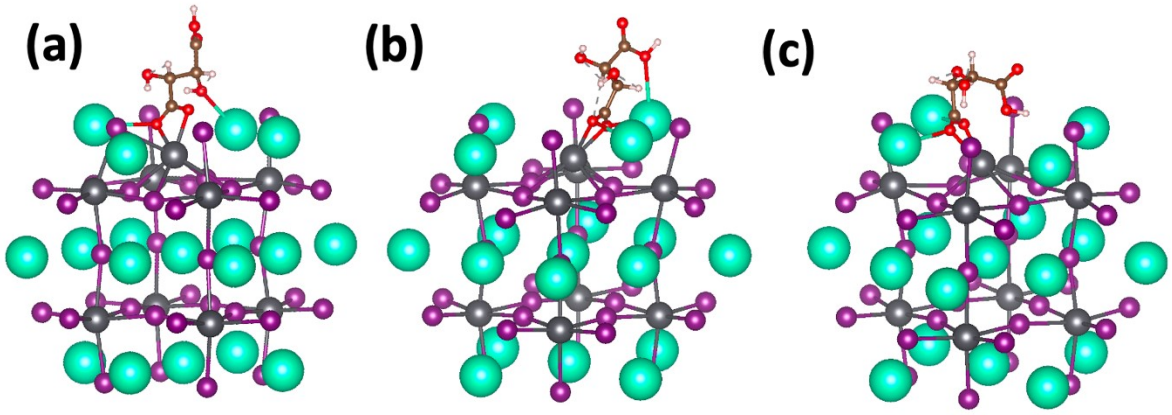

Figure S13: Pb-rich CsPbI3 cluster with tartarate binding to the surface Pb defect with initial conditions of the **(a)** trans, **(b)** gaunche(-), and **(c)** gaunche(+) conformations.

Table S4: Optical gap and ground-state electric dipole for the $CsPbI_3$ cluster and with the Lactic Acid series molecules bound to the surface in various conformations.

		Dihedral Angle (θ)	E_gap(eV)	static dipole(GS)	dip_x	dip_y	dip_z
CsPbI3 Cluster	**Pristine**	x	4.29	0.04	-0.04	0.00	0.00
CsPbI3 Cluster + (S) Lactic	**1-L**	x	4.27	3.44	1.92	2.32	1.66
	2-L	x	4.22	8.61	7.69	-2.94	-2.51
	3-L	x	4.24	6.92	6.91	0.05	-0.21
CsPbI3 Cluster + (S) Malic	**1-M**	0.15	4.22	10.30	9.52	3.35	2.10
	2-M	4.05	4.25	5.98	4.83	1.75	3.06
	3-M	27.86	4.24	9.92	8.71	-0.56	-4.70
	4-M	24.16	4.29	4.71	4.67	-0.52	0.31
	5-M	121.69	4.30	8.68	7.90	3.60	-0.14
	6-M	123.56	4.29	8.31	7.79	2.77	0.76
CsPbI3 Cluster + (S,S) Tartaric	**1-T**	2.67	4.24	8.61	8.32	-1.22	-1.85
	2-T	24.44	4.27	8.30	8.17	-0.45	-1.41
	3-T	121.37	4.29	11.32	10.68	3.71	0.36

Table S5: Relative energies and Boltzmann weights for various conformations of chiral molecules on the CsPbI3 surface.

		relative E (eV)	Boltzmann	Z	Fraction
(S) Lactic	1	0.172	0.00	1.65	0.00
	2	0.000	1.00		0.61
	3	0.011	0.65		0.39
(S) Malic	1, trans	0.211	0.00	1.02	0.00
	2, trans	0.219	0.00		0.00
	1, gaunche-	0.210	0.00		0.00
	2, gaunche-	0.394	0.00		0.00
	1, gaunche+	0.000	1.00		0.98
	2, gaunche+	0.109	0.02		0.01
(S,S) Tartaric	1, trans	0.067	0.08	1.08	0.07
	1, gaunche-	0.207	0.00		0.00
	1, gaunche+	0.000	1.00		0.93

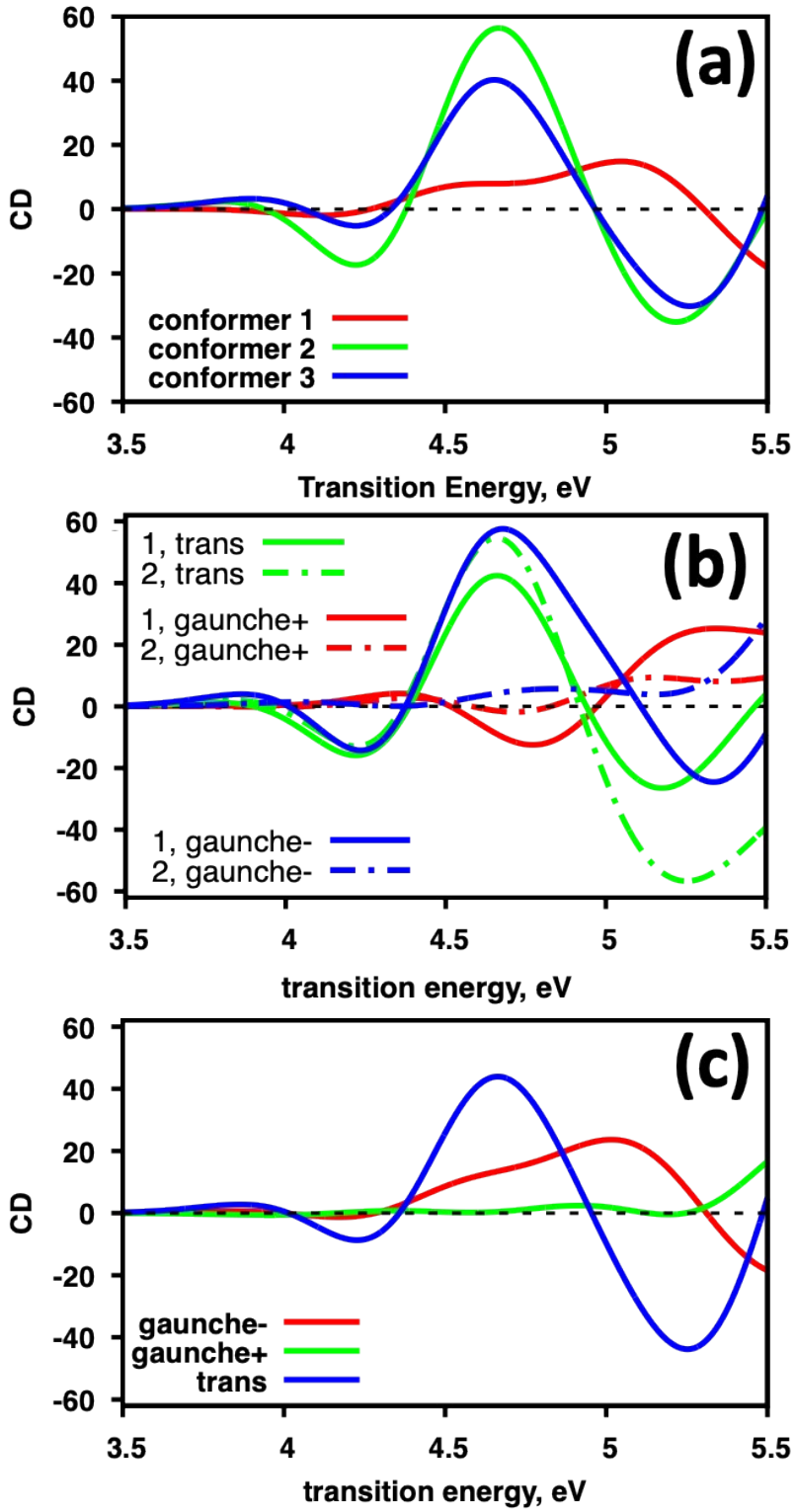

Figure S14: Circular dichroism spectra for **(a)** lactate, **(b)** malate, and **(c)** tartarate conformers bound to an excess Pb^{2+} ion on the CsPbI3 cluster surface.

Table S6: Comparing rotatory strength of for the S_1 excited state and root-mean-square for all excited states of rotatory strengths of the isolated molecule to the root-mean-square for all excited states of the combined system.

		Dihedral Angle (θ)	R_{S1}, cgs	RMS(R)		RMS(R)
(S) Lactate	1-L	x	3.79	15	**CsPbI3 Cluster + (S) Lactate**	182
	2-L	x	16.47	19		243
	3-L	x	11.57	12		199
(S) Malate	**1-M**	0.15	4.67	17	**CsPbI3 Cluster + (S) Malate**	226
	2-M	4.05	-3.19	12		238
	3-M	27.86	5.85	25		233
	4-M	24.16	-4.05	24		120
	5-M	121.69	-6.69	13		209
	6-M	123.56	-4.90	9		152
(S,S) Tartarate	**1-T**	2.67	8.32	19	**CsPbI3 Cluster + (S,S) Tartarate**	229
	2-T	24.44	17.13	24		175
	3-T	121.37	-4.17	15		97